ChemComm

Structural Conversion of Hunan Islet Amyloid Polypeptide Aggregates Under Electric Field

Journal:	*ChemComm*
Manuscript ID	CC-COM-06-2020-004466.R2
Article Type:	Communication

SCHOLARONE™
Manuscripts

Please do not adjust margins

Journal Name

ARTICLE

Structural Conversion of Hunan Islet Amyloid Polypeptide Aggregates Under Electric Field

Received 00th January 20xx,
Accepted 00th January 20xx

DOI: 10.1039/x0xx00000x

www.rsc.org/

Yongxiu Song[a,b#], Rongrong Wu[a#], Yin Wang[b], Lei Liu[a]* and Mingdong Dong[b]*

Electric field (EF) in biological system is well existing, which implies in the activity of protein ion channels and pumps in the varieties of cell. The aggregation of islet amyloid polypeptide (IAPP) is found in brain tissue recently and related to the electrical activity of neurons and cause neuronal loss. However, the association between amyloid formation and electric field is still unknown. Herein we report an direct method to stimulate the formation of hIAPP peptide under EF.

Environmental factors, such as light, physical perturbations, heat, pH, ionic concentration and electric field/magnetic field, have a great impact on protein aggregation, which could mediate the biological functions or even related to the pathogenesis of disease.[1,2] Recently, the consequence on protein functionality from electric field attracts a great attention.[3] For instance, the bioelectric field exists well in human body, specifically in brain neurons.[4] The action potential generated around the neurons is approximately determined to be -70 mV to 40 mV, with the EF intensity of 2 mV/nm to 3.5 mV/nm.[5] The assembly pathway of protein especially for amyloid protein existing in the microenvironment could be mediated. Therefore, it is important to the understanding the structure of amyloid protein aggregation under EF. In the most studies, Amyloid β (Aβ) is considered to be the protein existing at the extracellular environment in the brain, and the aggregation is closely related to the pathogenesis of AD.[6] However, in recent, hIAPP is also found in the brain, and it is reported that the dementia is one possible complication of Type 2 diabetes(T2DM).[7] Therefore, it is meaningful and critical to investigate the hIAPP assembled structure under EF.

The great efforts have been made to control the peptide assembly by setting up a device with the defined electric field with relative high range of potencial.[8] In this work, a simulated bioelectric field was set up to explore the aggregation and induced structure of hIAPP at the defined environment (Fig 1a). To simulate the electric field between the neurons, different EF intensity (0 mV/nm, 0.001 mV/nm, 0.002 mV/nm, 0.003 mV/nm) was defined according to electric field range. β-sheet secondary structure of hIAPP converted into non-β sheet structure under electric field, which is verified by experiments and theoretical simulation.

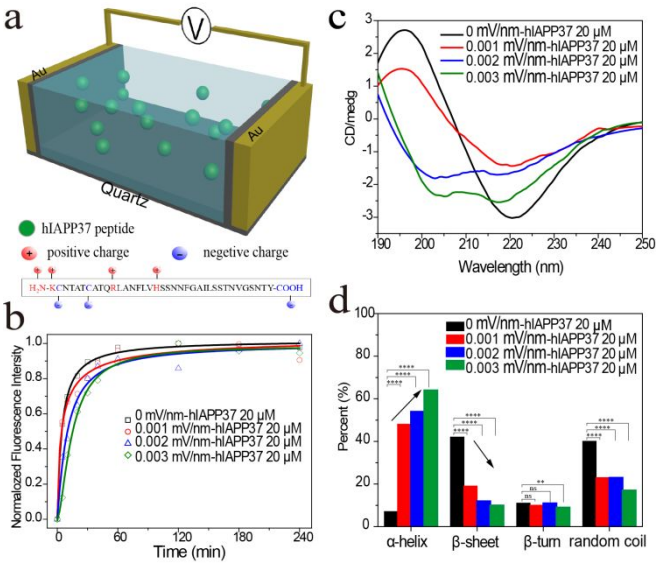

Fig 1 (a) Scheme of electric field effect on aggregation process of hIAPP37 peptide; (b) Aggregation kinetic of hIAPP37 peptide under EF (0 mV/nm, 0.001 mV/nm, 0.002 mV/nm, 0.003 mV/nm); (c) Circular dichroism spectra of hIAPP37 peptide (20 μM) under EF (0 mV/nm, 0.001 mV/nm, 0.002 mV/nm, 0.003 mV/nm); (d) The content of corresponding secondary structure in (c); One-way analysis of variance (ANOVA) with Tukey's correction, not significant (n.s.), **P < 0.01, ****P < 0.0001.

[a] *Institute for Advanced Materials, Jiangsu University, China. E-mail: liul@ujs.edu.cn*
[b] *Interdisciplinary Nanoscience Center (iNANO), Aarhus University, Aarhus, Denmark, Email: dong@inano.au.dk*
[#] *These authors contributed equally*

† Footnotes relating to the title and/or authors should appear here.
Electronic Supplementary Information (ESI) available: [details of any supplementary information available should be included here]. See DOI: 10.1039/x0xx00000x

Please do not adjust margins

Initially, we tested the aggregation of hIAPP37 peptide with the effect of different electric field intensity (0 mV/nm, 0.001 mV/nm, 0.002 mV/nm, 0.003 mV/nm). Thioflavin T(ThT) fluorescence assay is used as a techque to detect the kinetic of peptide aggregation based on fluorescence signals resulting from ThT binding to β-sheet structure.[9] As seen in Fig 1b and Fig S1, hIAPP37 peptide displayed a similar kinetic of aggregation process in the absence or presence of electric field. However, the aggregation rate of hIAPP37 peptide was reduced in the absence or presence of EF. However, the aggregation rate of hIAPP37 was reduced under the EF, moreover, the inhibition of peptide aggregation became more obviously with the increase of EF intensity, which indicates the affection of EF on β-sheet secondary structure of hIAPP. Circular dichroism (CD) spectra (Fig 1c) further verified it. Consistently with ThT assay results, the secondary structure of hIAPP37 was regulated from a typical β-sheet structure showing a broad negative peak at around 220 nm and a positive peak at 198 nm (black curve in Fig 1c) (without EF) to a stable helical structure with two negative peaks at around 217 nm and 205 nm under low EF intensity (0.002 mV/nm and 0.003 mV/nm).[10,11]

Meanwhile, the content of secondary structures of hIAPP37 aggregates was calculated by using DichroWeb online software,[12] as shown in Fig 1d. It is found that the EF could facilitate α-helix increasing (from 7% to 64%) and β-sheet and random coil conformation decreasing (from 42% and 40% to 10% and 17%, respectively) compared with the one of hIAPP aggregates without EF

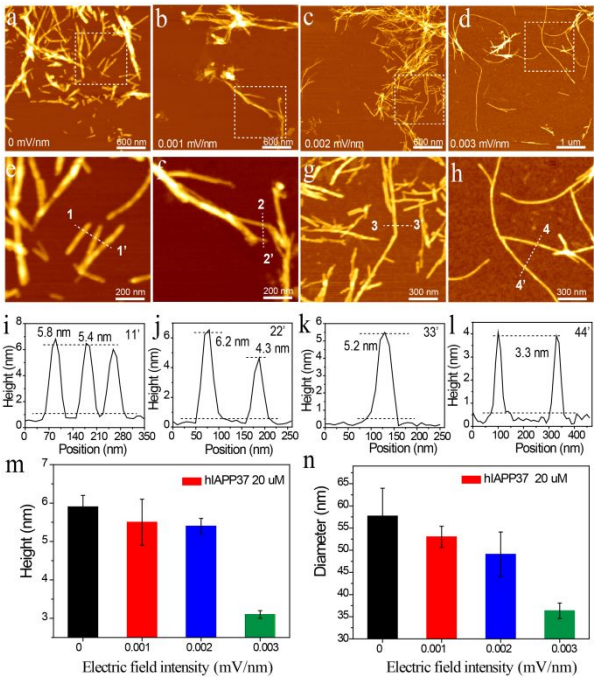

Fig 2 The morphologies of hIAPP37 (20 μM) aggregates with or without EF. The morphology of hIAPP37 aggregates with EF intensity of 0 mV/nm (a), 0.001 mV/nm (b), 0.002 mV/nm (c), and 0.003 mV/nm (d); (e) AFM image zoomed from Fig 2(a); (f) AFM image zoomed from Fig 2(b); (g) AFM image zoomed from Fig 2(c); (h) AFM image zoomed from Fig 2(d); (i) The height line-profile of 11' in Fig 2(e); (j)The line profile of 22' in Fig 2(f); (k) The line profile of 33' in Fig 2(g); (l) The line profile of 44' in Fig 2(h); (m) The histogram with Gaussian fitting of the height distribution of morphologies of hIAPP37 aggregates in 2(a-d); (n) The histogram with Gaussian fitting of the diameter distribution of morphologies of hIAPP37 aggregates in 2(e-h); The scale bar of images in Fig 2 (a, b, c) is 600 nm, the scale bar of AFM image in Fig 2(d) is 1um, the scale bar of images in Fig 2 (e,f) is 200 nm and the scar bar of images in Fig 2 (k,l) is 300 nm.

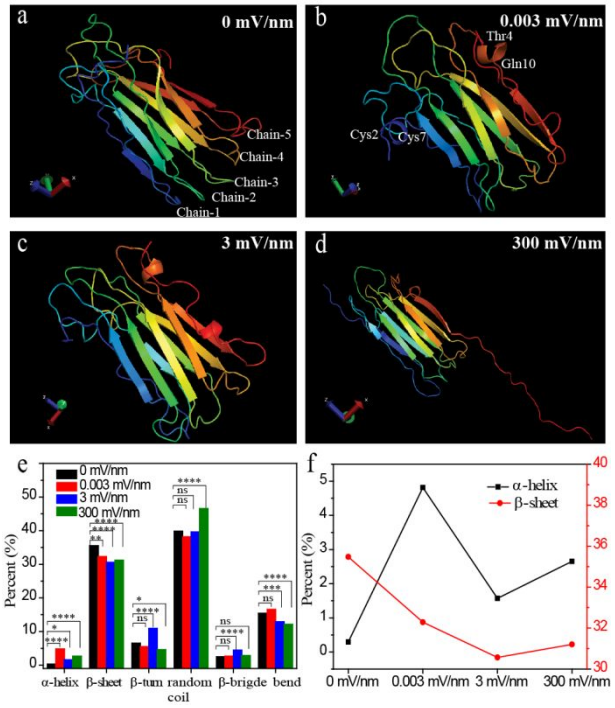

Fig 3 The morphology and secondary structure of hIAPP37 pentamer under EF. (a) Conformation of hIAPP37 pentamer aggregates with the electric field intensity of 0 mV/nm(a), 0.003 mV/nm(b), 3 mV/nm(c), and 300 mV/nm(d), obtained from AAMD simulations at t=300 ns; (e) the corresponding secondary structural populations of hIAPP37 pentamer aggregates under electric fields (0 mV/nm, 0.003 mV/nm, 3 mV/nm, and 300 mV/nm) . (f) The corresponding plot of the content of α-helix and β-sheet structure in Fig 3(e); One-way analysis of variance (ANOVA) with Tukey's correction, not significant (n.s.), *P < 0.05, **P < 0.01, ***P < 0.001, ****P < 0.0001.

applied. In addition, the EF could further have the affection on the morphology of hIAPP37 aggregates. Many thick fibrils and fibril cluster of hIAPP37 were observed by AFM, with the determined height of 5.9 ± 0.3 nm (Fig 2(a, e), line-profile 11' in Fig 2i). With the EF applied (0.001 mV/nm, 0.002 mV/nm, 0.003 mV/nm), the amyloid fibril converted into thin and long filaments, and the heights and diameters of hIAPP fibrils decreased with the increment of EF (Fig 2 (b-d, f-h, m-n)). Based on aggregation behaviour test, secondary structure analysis and morphology characterization of hIAPP aggregates with the EF applied, we can conclude that electric field do affect the self-assembly of hIAPP which is mainly due to the molecular interaction regulation between peptides.

To further gain insight into the secondary structure transition and molecular mechanism of hIAPP37 peptide under electric field, all-atom molecular dynamics (AAMD) simulations was carried out on the hIAPP pentamer with β-sheet-rich structure under different EF intensities. Different EF intensity (0 mV/nm, 0.003 mV/nm, 3 mV/nm, 300 mV/nm) in simulations is defined to explore the different effects of low and high EF intensity on hIAPP37 self-assembly. The convergence and stability of the simulation was evaluated before data collection and analysis (Fig S2). It is found that hIAPP37 pentamer is extremely stable with β-sheet-rich structure under low EF intensity.[13] The representative structure conformations of hIAPP pentamer at the end of simulation (t = 300 ns) were shown in Fig 3(a-d). In case of low EF intensity of 0.003

This journal is © The Royal Society of Chemistry 20xx

mV/nm and 3 mV/nm, we obviously observed the formation of helical structure at chain-1 and chain-5 with cysteine (C2 and C7), threonine(T4) and glutamine (Q10) exposed outside the helical structure (Fig 3(b, c)). β-strand stretches along the axis of EF, especially in high EF intensity (Fig 3d).[14] More random coil conformation is formed in this case compared with the structure without EF applied. It is consistent with the results in Fig 3e, that noticeable reduction of random coil and β-sheet is found, while the content of α-helix is increasing at t = 300 ns under the EF intensity of 0.003 mV/nm and 3 mV/nm (Fig 3e). However, with the EF intensity of further increased, random coil structure recover, meanwhile β-strand structure is restricted to align along the direction of EF, which facilitates the hIAPP pentamer to be tidiness. The noticeable difference is revealed compared with hIAPP37 pentamer without EF applied and it has a similar trend of the secondary structure conversion of hIAPP37 pentamer under low EF intensity with that in experiments, while, little fluctuation exists in secondary structure of hIAPP37 pentamer (Fig 3f and Fig S4) under high EF intensity (300 mV/nm) which runs for 3 times in the same condition, indicating the structure of hIAPP37 pentamer is unstable under high EF.

The secondary structure variation is resulted from the mediated interaction between the peptides, as well as peptide and water molecular. We evaluated the total energy, coulomb energy and vdW interaction energy in different cases (Fig S3(a)), and there is no obvious variation, but slight variation exists in the hydrogen bonds (HBs) among peptides, peptide and water molecular (Fig S3(b, c)). Under the EF, both HBs of intra protein and protein-water increase slightly, which implies the structure of hIAPP pentamer is stable.[15]

To further reveal the mechanism of the mediated interaction between peptides under EF, the intramolecular and intermolecular contact map of hIAPP37 pentamer are studied, as shown in Fig 4. The probability of interpeptide (or intrapeptide) contact between different pairs of amino acid residues during peptide self-assembly could be visualized in contact map, which is used to analyze the interactions between amino acid residues in peptides.[16] Fig 4(a-b) are symmetrically with the right diagonal of 0 nm and the distance of 1.5 nm in contact maps indicates that there is no contact between residues. In Fig 4 (a-b , d-e), the smaller the distance between residues, the greater the contact strength. Fig 4a shows the intrapeptide contacts between the same pairs of amino acid residues and pairwise contacts, R11 and hIAPP30-37 fragment, F15 and hIAPP20-30 fragment among which presents the prominent closely contact, indicating the interaction between these two fragments might be liable to mediate. With EF applied, the residues contact in intrapeptide was modulated (Fig 4b), and the interaction difference in intrapeptide with EF intensity (0mV/nm and 0.003 mV/nm) could be revealed by the contact difference map (Fig 4c). In Fig 4 (c,f), light green (0 nm) means the contact distance between residues does not change under the effect of EF (0.003 mV/nm); dark red (> 0 nm) and dark blue (< 0 nm) severally indicate that the contact distance become longer and closer under the effect of EF (0.003 mV/nm). The closer the contact distance, the stronger the interaction between residues, and vice versa. The contact between hIAPP5-8 fragment and hIAPP30-35 fragment became stronger, on the contrary, the red area showed that the contact between hIAPP13-16 fragment and hIAPP28-30 fragment became weaker. Moreover, the contact difference map of the interpeptide (Fig 4f) shows a similar trend among these 4 fragments based the contact map of interpeptides with or without EF (Fig 4d and 4e). The composition of these fragments are main polar and hydrophobic amino acids, such as cysteine(C), phenylalanine(F), tyrosine(Y), alanine(A), leucine(L), and valine(V),[17] which are more fragile to be mediated with EF applied. It is ascribed that the polarization of polar amino acids and side-chain arrangements, resulting from molecular dipoles of polar amino acids directly modulated with EF applied. [14,16,18] Furthermore, it is easy from Fig 4c and Fig 4f to find the distance between the N-terminus and hIAPP30-35 fragment become closer, in contrast, the distance between R11 and hIAPP30-37 fragment is more far away. The contact difference is originated from the interaction modulation between peptides under EF. The H bonds and interactions between these peptides are liable to modulate, which might further regulate

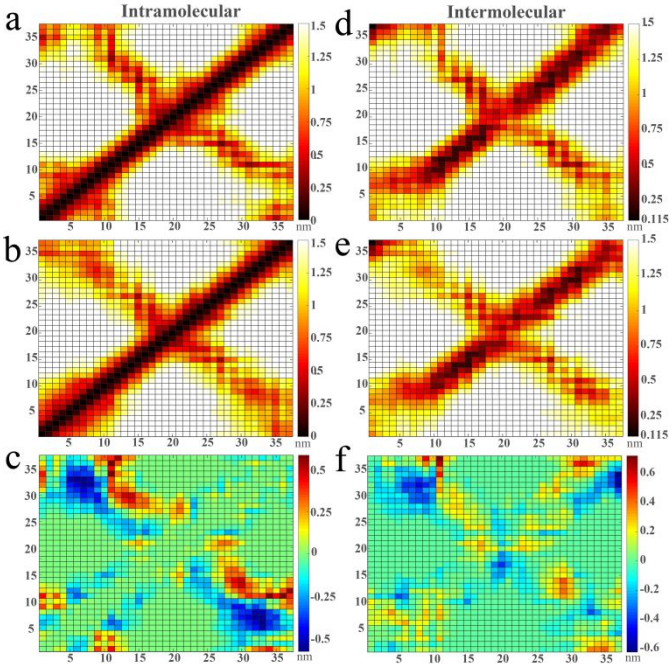

Fig 4 Residues contact map of hIAPP37 pentamer , both the x and y axes have the residues number in the peptide hIAPP37 sequence. (a-b) and (d-e) represent the intramolecular and intermolecular residues contact map under the EF strength of 0mV / nm and 0.003mv/nm, respectively. The color bar shows the average contact strength between residues of hiapp37 pentamer. (c) Intramolecular contact difference map of (a) and (b); (f) Intermolecular contact difference map of (d) and (e); This color bar represents the variation of residues contact strength. Fig 4(a-c) are symmetric with respect to the diagonal, whereas Fig 4(d-f) not.

the secondary conformation of hIAPP. The simulation results are consistent with tested results of hIAPP37 peptide under the EF intensity of 0.003 mV/nm in experiment.

In summary, we have investigated the effect of electric field on the self-assembly of hIAPP37 by experimental and theoretical studies. The experimental observations reveal that the increase of α-helix conformation accompany with the reduction of β-sheet and random coil, resulting in long and thin hIAPP37 fibrils under the EF. MD simulation verified the conformation transition of hIAPP37 pentamer from β-sheet to non-β-sheet under EF which is mainly due to the mediated interaction of interpeptide and intrapeptide especially from the polar and charged residues in hIAPP37. The

findings in this work may shed light on the affection of bioelectric field around neurons on the self-assembly of amyloid peptides, which will advance the understanding of pathogenesis of amyloid related disease and the potential for new treatment.

This work was supported by grants from the Independent Research Fund Denmark, European Union's Horizon 2020 (MNR4SCELL no. 734174), Carlsberg Foundation, National natural science foundation (21573097, 51503087).

Conflicts of interest

There are no conflicts to declare

Notes and references

1. a) W. Wang, S. Nema and D. Teagarden, *Int. J. Pharm*., 2010, **390**, 89; b) M. Jucker and L. C. Walker, *Nat. Neurosci*., 2018, **21**, 1341; c) S. Jha, J. M. Snell, S. R. Sheftic, S. M. Patil, S. B. Daniels, F. W. Kolling and A. T. Alexandrescu, *Biochemistry*., 2014, **53**, 300.
2. a) W. Wang, N. Li and S. Speaker, *Aggreg. Therap. Prot*., 2010, **119**; b) L. Liu, L. H. Klausen and M. D. Dong, *Nano. Today.*, 2018, **23**, 40; c) L. J. Martin, B. Akhavan and M. M. M. Bilek, *Nat. Commun*., 2018, **9**, 357.
3. a) E. De Genst, A. Messer and C. M. Dobson, *BBA-Proteins Proteom*., 2014, **1844**, 1907; b) R. M. Rodrigues, A. A. Vicente, S. B. Petersen and R. N. Pereira, *Innov. Food. Sci. Emerg*., 2019, **52**, 1; c) G. Wei, Z. Su, N. P. Reynolds, P. Arosio, I. W. Hamley, E. Gazit and R. Mezzenga, *Chem. Soc. Rev*., 2017, **46**, 4661.
4. a) X. Duan, T. M. Fu, J. Liu and C. M. Lieber, *Nano Today.*, 2013, **8**, 351; b) M. Lv, C. Wang, G. Ren, J. Ma and X. Song, *Nonlinear Dynam*., 2016, **85**, 1479; c) F. Wu, J. Ma and G. Zhang, *Appl. Math. Comput*., 2019, **347**, 590.
5. a) J. J. Palop and L. Mucke, *Nat. Neurosci.*, 2010, **13**, 812; b) G. S. Bloom, *Jama Neurol.*, 2014, **71**, 505.
6. a) C. Cheignon, M. Tomas, D. Bonnefont-Rousselot, P. Faller, C. Hureau and F. Collin, *Redox Biol.*, 2018, **14**, 450; b) F. Panza, M. Lozupone, G. Logroscino and B. P. Imbimbo, *Nat. Rev. Neurol.*, 2019, **15**, 73; c) L. Liu, L. Niu, M. Xu, Q. Han, H. Duan, M. D. Dong, F. Besenbacher, C. Wang and Y. Yang, *ACS Nano*, 2014, **8**, 9503; d) T. Wang, L. Zhang, J. Wang, Y. Feng, E. Xu, X. Mao and L. Liu, *Chem. Commun.*, 2018, **54**, 13084.
7. a) L. A. Mohamed, H. Zhu, Y. M. Mousa, E. Wang, W. Q. Qiu and A. Kaddoumi, *J. Alzheimers Dis.*, 2017, **56**, 1087; b) P. Liu, S. Zhang, M. L. Chen, Q. Liu, C. Wang, C. Wang, Y. M. Li, F. Besenbacher and M. D. Dong, *Chem. Commun.*, 2012, **48**, 191; c) L. Zhang, Q. Chen, P. Li, L. Yuan, Y. Feng, J. Wang, X. Mao and L. Liu, *Chem. Commun*., 2019, **55**, 14359; d) D. Mauricio, N. Alonso and M. Gratacos, *Trends. Endocrin. Met*., 2020, **31**, 287.
8. J. Saikia, G. Pandey, S. Sasidharan, F. Antony, H. B. Nemade, S. Kumar, N. Chaudhary and V. Ramakrishnan, *Acs Chem. Neurosci*., 2019, **10**, 2250;
9. G. Shanmugam and P. L. Polavarapu, *Biophys. J*., 2004, **87**, 622.
10. N. Sreerama and R. W. Woody, *Method. Enzymol.*, 2004, **383**, 318.
11. N. J. Greenfield, *Trends. Anal. Chem.*, 1999, **18**, 236.
12. a) L. Whitmore and B. A. Wallace, *Nucleic Acids Res.*, 2004, **32**, W668; b) A. Lobley, L. Whitmore and B. A. Wallace, *Bioinformatics.*, 2002, **18**, 211.
13. G. Liang, J. Zhao, X. Yu and J. Zheng, *Biochemistry*, 2013, **52**, 1089.
14. T. Stuyver, D. Danovich, J. Joy and S. Shaik, *Wires. Comput. Mol. Sci*., 2020, **10**, e1438.
15. a) R. Xing, C. Yuan, S. Li, J. Song, J. Li and X. Yan, *Angew. Chemie.Int. Ed.*, 2018, **57**, 1537; b) M. Amit, S. Yuran, E. Gazit, M. Reches and N. Ashkenasy, *Adv. Mater*., 2018, **30**, 1707083.
16. F. Lugli, F. Toschi, F. Biscarini and F. Zerbetto, *J. Chem. Theory.Comput*., 2010, **6**, 3516.
17. a) F. Morcos, A. Pagnani, B. Lunt, A. Bertolino, D. S. Marks, C. Sander, R. Zecchina, J. N. Onuchic, T. Hwa and M. Weigt, *Proc. Natl. Acad. Sci. U.S.A.*, 2011, **108**, E1293; b) P. Zhang, Z. Wang, L. Liu, L. H. Klausen, Y. Wang, J. Mi, M. Dong, *Appl. Mater. Today*, 2019, 14, 151-158.
18. Q. Xiong, Y. Jiang, X. Cai, F. Yang, Z. Li and W. Han, *Acs Nano*., 2019, **13**, 4455.

This journal is © The Royal Society of Chemistry 20xx

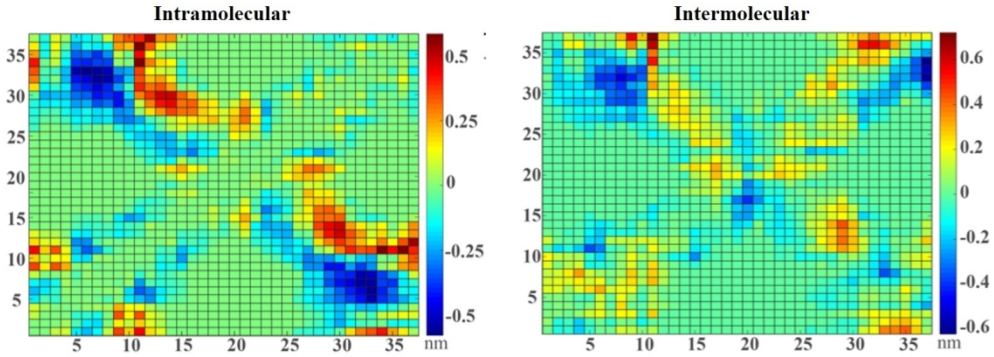

269x98mm (150 x 150 DPI)